Supporting Information

Deflecting lithium dendritic cracks in multi-layered solid electrolytes

Bingkun Hu[1], Shengming Zhang[1], Ziyang Ning[1,2], Dominic Spencer-Jolly[1,3], Dominic L.R. Melvin[1], Xiangwen Gao[1,4], Johann Perera[1], Shengda D. Pu[1], Gregory J. Rees[1], Longlong Wang[1], Lechen Yang[1], Hui Gao[1], Shashidhara Marathe[5], Genoveva Burca[5,6,7], T. James Marrow[1]*, & Peter G. Bruce[1,8,9]*

1. Department of Materials, University of Oxford, Oxford, UK

2. Fujian Science & Technology Innovation Laboratory for Energy Devices (21C Lab), Ningde, China

3. School of Metallurgy and Materials, University of Birmingham, Birmingham, UK

4. Future Battery Research Center, Global Institute of Future Technology, Shanghai Jiao Tong University, Shanghai, China

5. Diamond Light Source, Harwell Campus, Didcot, UK

6. STFC-Rutherford Appleton Laboratory, ISIS Facility, Harwell, UK

7. Faculty of Science and Engineering, The University of Manchester, UK

8. Department of Chemistry, University of Oxford, Oxford, UK

9. Lead contact

*Correspondence: peter.bruce@materials.ox.ac.uk; james.marrow@materials.ox.ac.uk

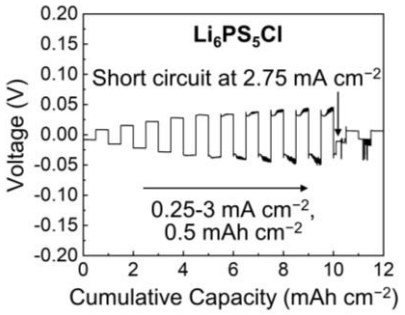

Figure S1. The voltage profile of a Li/Li_6PS_5Cl/Li cell cycled at stepwise increasing current density from 0.25–3 mA cm^{-2} under 2.5 MPa. The current step is 0.25 mA cm^{-2} and the plating/stripping capacity is 0.5 mAh cm^{-2} per half cycle. The cell short-circuits at 2.75 mA cm^{-2}.

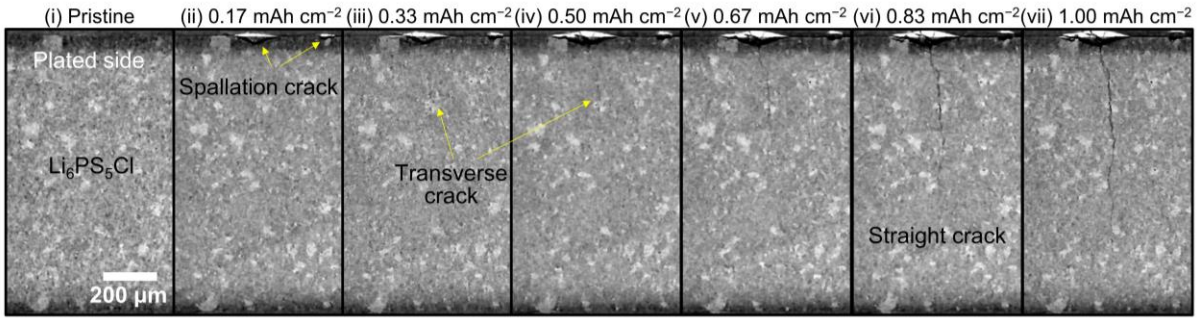

Figure S2. XCT virtual cross-sections of a Li/Li_6PS_5Cl/Li cell before plating (i), and after plating 0.17 (ii), 0.33 (iii), 0.50 (iv), 0.67 (v), 0.83 (vi), 1.00 mAh cm^{-2} (vii). It is observed that the crack propagates through the monolithic electrolyte without deflection.

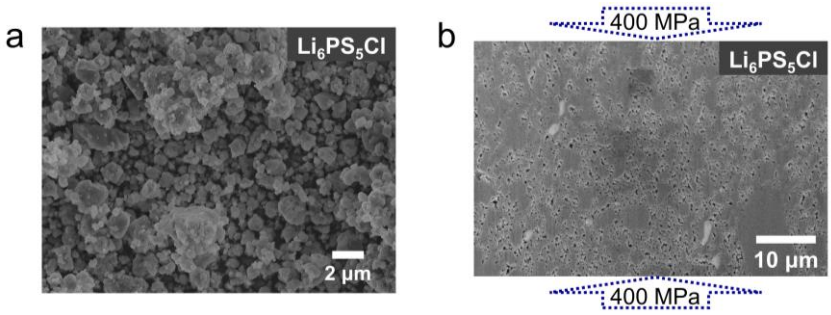

Figure S3. Morphological characterisation of Li_6PS_5Cl. a, SEM image of pristine Li_6PS_5Cl powder. **b,** PFIB-SEM image of pressed Li_6PS_5Cl disc. The uniaxial pressure applied to the electrolyte during fabrication is indicated by blue arrows.

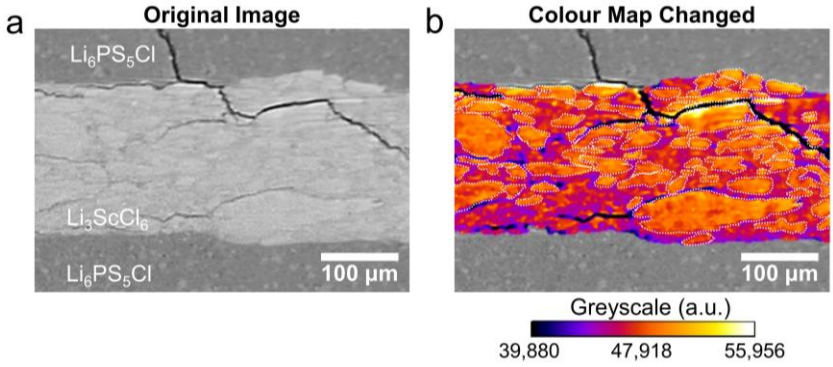

Figure S4. A comparison of the XCT image in Figure 3a with and without the colour map overlay. a, The original XCT cross-section. **b,** The same cross-section after overlaying the colour map of the Li_3ScCl_6 region to highlight the microstructural inhomogeneity.

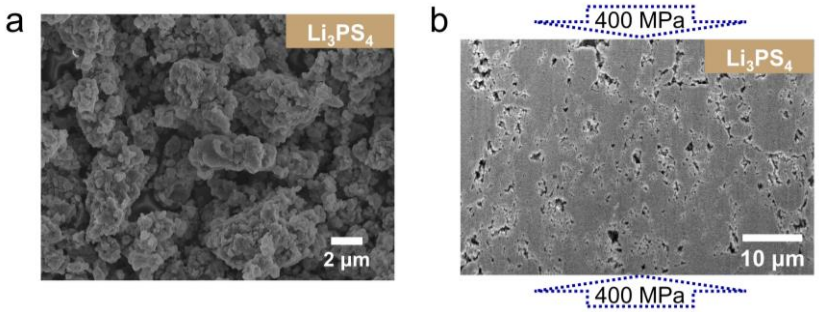

Figure S5. Morphological characterisation of Li_3PS_4. a, SEM image of pristine Li_3PS_4 powder. **b,** PFIB-SEM image of pressed Li_3PS_4 disc. The uniaxial pressure applied to the electrolyte during fabrication is indicated by blue arrows.

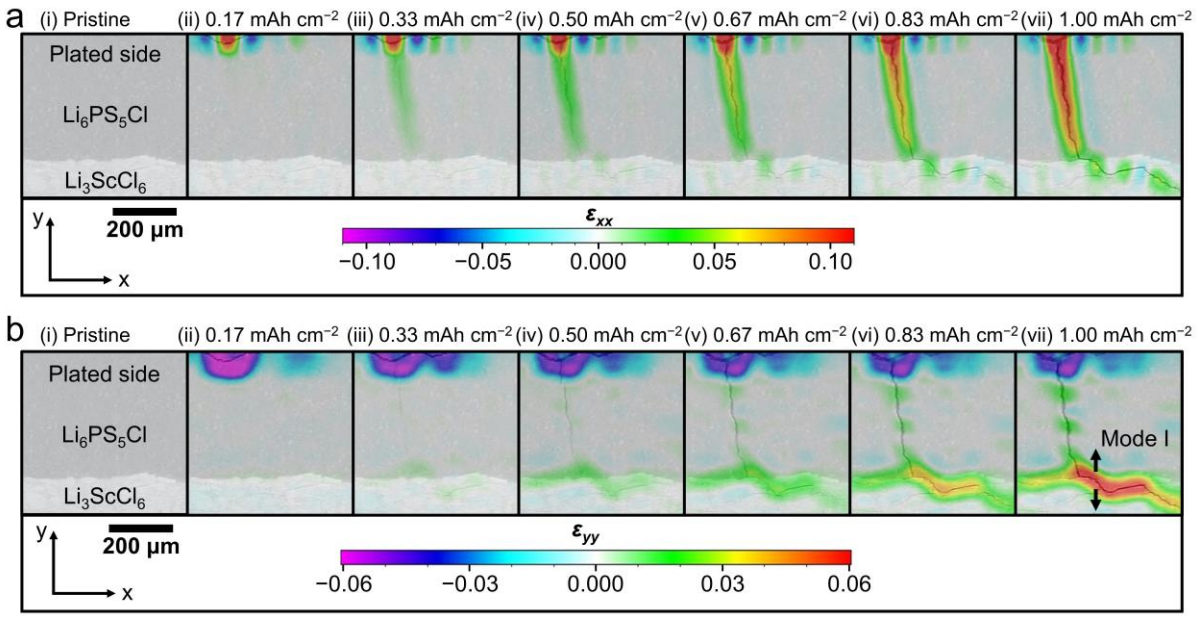

Figure S6. Maps of normal strain of the Li/Li_6PS_5Cl/Li_3ScCl_6/Li_6PS_5Cl/Li cell, obtained from DVC analysis of the XCT scans. a, ε_{xx}. b, ε_{yy}.

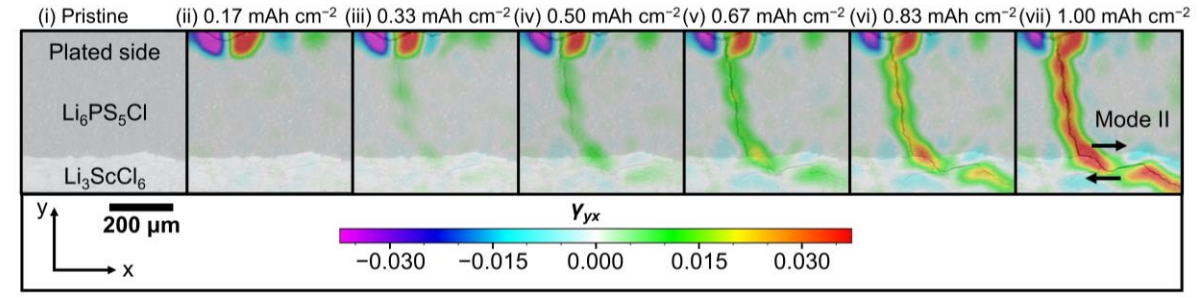

Figure S7. Maps of shear strain γ_{xy} of the Li/Li_6PS_5Cl/Li_3ScCl_6/Li_6PS_5Cl/Li cell, obtained from DVC analysis of the XCT scans.

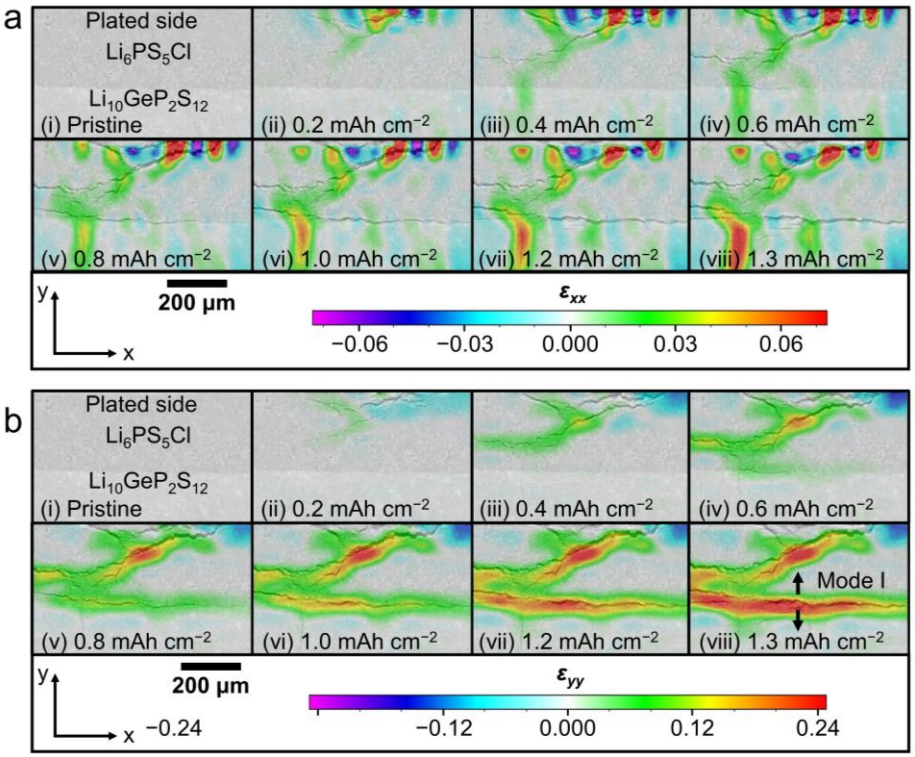

Figure S8. Maps of normal strain of the Li/Li_6PS_5Cl/$Li_{10}GeP_2S_{12}$/Li_6PS_5Cl/Li cell, obtained from DVC analysis of the XCT scans. a, ε_{xx}. b, ε_{yy}.

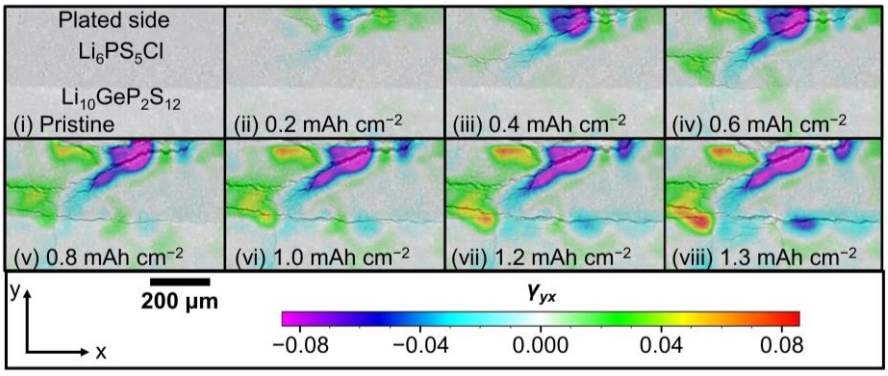

Figure S9. Maps of shear strain γ_{xy} of the Li/Li_6PS_5Cl/$Li_{10}GeP_2S_{12}$/Li_6PS_5Cl/Li cell, obtained from DVC analysis of the XCT scans.

Table S1. The mean roughness of the entire interface between the main solid electrolyte and the inner layer, calculated using XCT image stacks which include the whole interface.

Solid electrolyte	Li_6PS_5Cl/Li_3ScCl_6/ Li_6PS_5Cl	Li_6PS_5Cl/$Li_{10}GeP_2S_{12}$/ Li_6PS_5Cl	Li_6PS_5Cl/Li_3PS_4/ Li_6PS_5Cl
Roughness, R_a (µm)	6.63	5.37	5.93

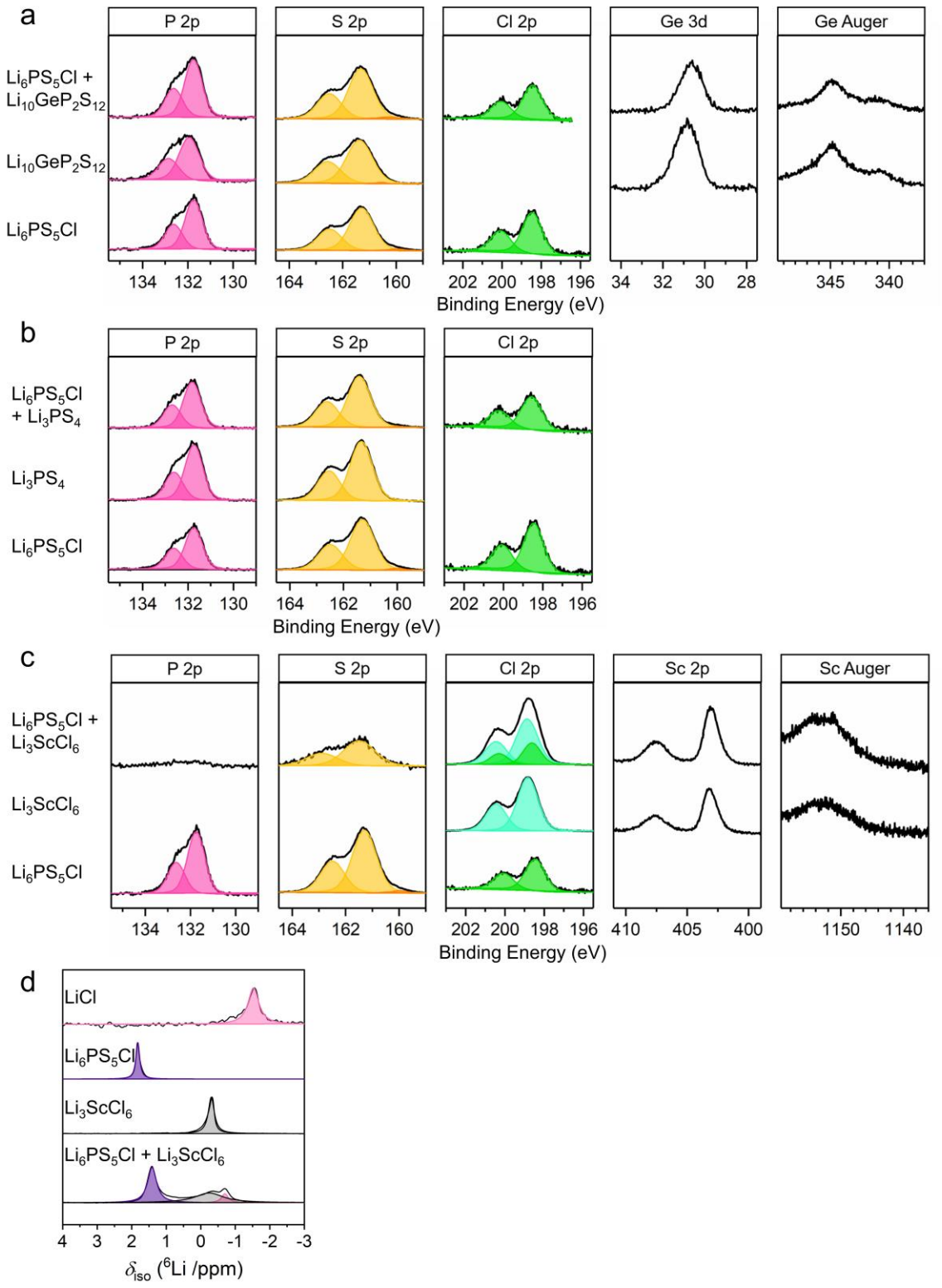

Figure S10. Interfacial chemical reaction characterised by X-ray photoelectron spectroscopy (XPS) and nuclear magnetic resonance (NMR) spectroscopy. a, XPS results of the $Li_6PS_5Cl/Li_{10}GeP_2S_{12}$ mixed powders. **b,** XPS results of the $Li_3PS_4/Li_{10}GeP_2S_{12}$ mixed powders. **c,** XPS results of the Li_6PS_5Cl/Li_3ScCl_6 mixed powders. **d,** ^6Li NMR results of the Li_6PS_5Cl/Li_3ScCl_6 mixed powders.

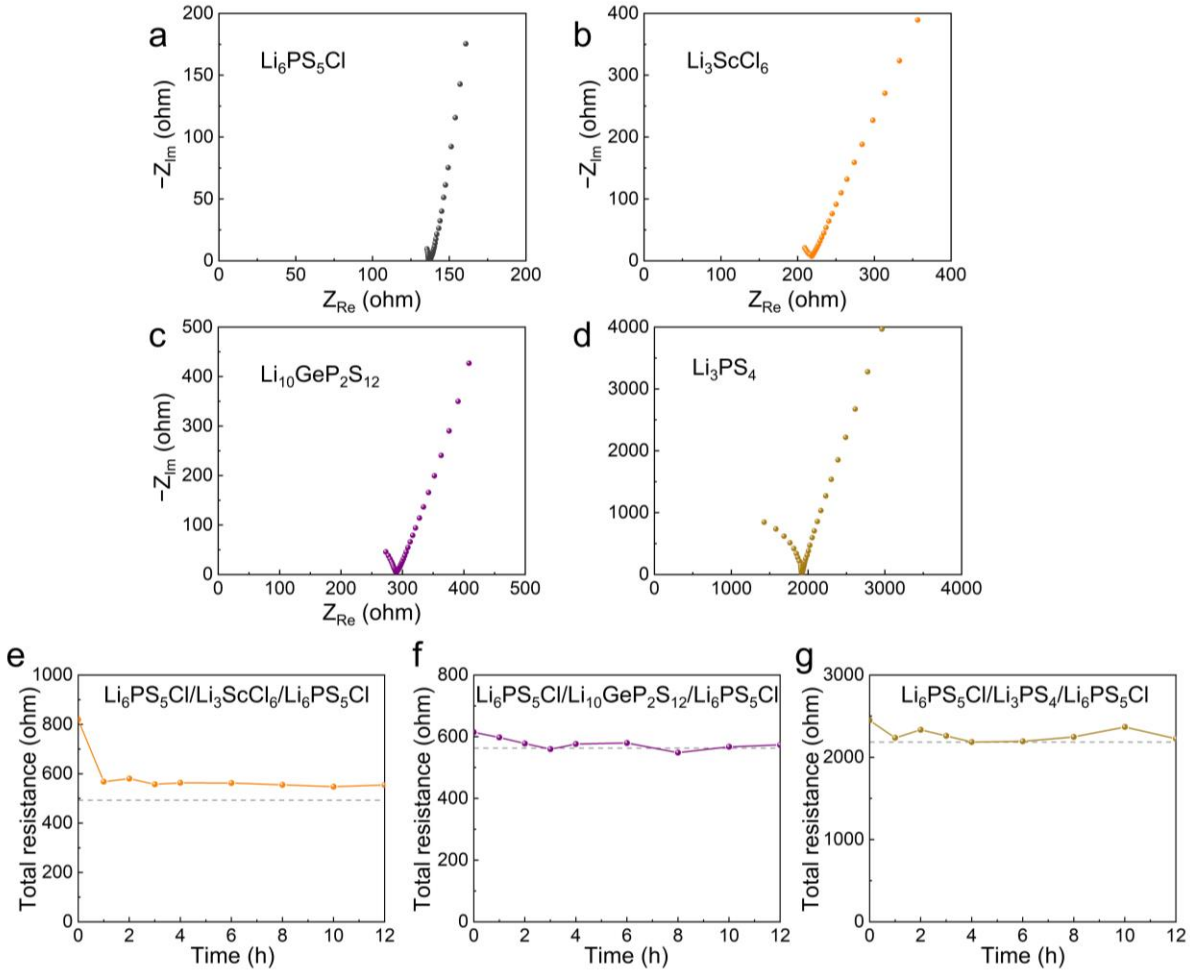

Figure S11. Impedance evolution of multi-layered samples. Impedance of discs composed of **a,** Li_6PS_5Cl, **b,** Li_3ScCl_6, **c,** $Li_{10}GeP_2S_{12}$ and **d,** Li_3PS_4. The variation in impedance of **e,** $Li_6PS_5Cl/Li_3ScCl_6/Li_6PS_5Cl$, **f,** $Li_6PS_5Cl/Li_{10}GeP_2S_{12}/Li_6PS_5Cl$, **g,** $Li_6PS_5Cl/Li_3PS_4/Li_6PS_5Cl$ over time. All cells are measured using blocking electrodes. The impedances of all multi-layered samples remain constant over rest time, and the values closely match the total impedances of the individual layers (indicated by dashed lines in e–g).

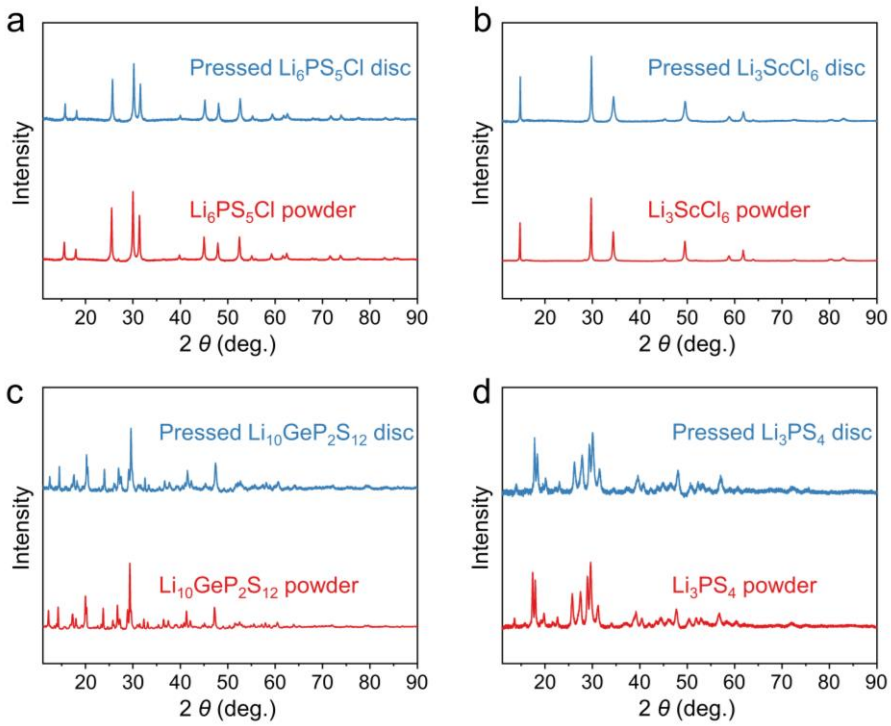

Figure S12. PXRD patterns of pristine solid electrolytes. PXRD patterns of pristine **a,** Li_6PS_5Cl, **b,** Li_3ScCl_6, **c,** $Li_{10}GeP_2S_{12}$ and **d,** Li_3PS_4 powders and after pressing into discs, no changes are observed on pressing.

Table S2. Measured porosity of Li_6PS_5Cl, $Li_{10}GeP_2S_{12}$, Li_3ScCl_6, and Li_3PS_4 solid electrolytes.

Sample	Li_6PS_5Cl	Li_3ScCl_6	$Li_{10}GeP_2S_{12}$	Li_3PS_4
Porosity	16.2%	15.5%	16.8%	15.9%